

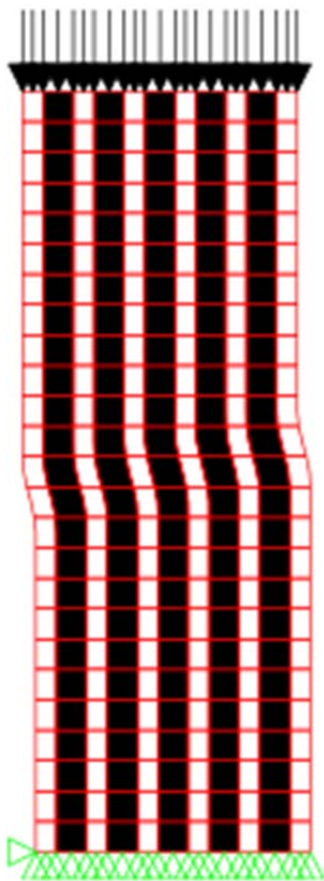


---

# COMPOSITE MATERIALS IN COMPRESSION

---

**Mechanical Engineering**  
Technical Report ME-TR-4



---

# DATA SHEET

**Title:** Composite materials in compression  
**Subtitle:** Mechanical Engineering  
**Series title and no.:** Technical report ME-TR-4

**Author:** Jens Lycke Wind  
Department of Engineering – Mechanical Engineering,  
Aarhus University

**Internet version:** The report is available in electronic format (pdf) at the Department of Engineering website  
<http://www.eng.au.dk>.

**Publisher:** Aarhus University©  
**URL:** <http://www.eng.au.dk>

**Year of publication:** 2013 Pages: 34  
**Editing completed:** January 2013

**Abstract:** A geometric and material non-linear finite element code is built using Matlab. The theoretical derivations for building the code is outlined and explained by pseudo code. Three different solvers are introduced; the Newton Raphson method, the modified Newton Raphson method, and the arc length method. The code is tested for material non-linearity an geometric non-linearity separately using standard reference solutions. The future work is outlined as a continuity of this report.

**Keywords:** Unidirectional composite, non-linear finite element method, kink-band formation, material instability

**Supervisor:** Henrik Myhre Jensen

**Please cite as:** Authors, year. Title. Department of Engineering, Aarhus University. Denmark. 34 pp. - Technical report ME-TR-4

**Layout:** LaTeX

**Cover photo/image:** Jens Lycke Wind

**ISSN:** 2245-4594

Reproduction permitted provided the source is explicitly acknowledged

---

# COMPOSITE MATERIALS IN COMPRESSION

Jens Lycke Wind

Aarhus University, Department of Engineering

## **Abstract**

---

A geometric and material non-linear finite element code is built using Matlab. The theoretical derivations for building the code is outlined and explained by pseudo code. Three different solvers are introduced; the Newton Raphson method, the modified Newton Raphson method, and the arc length method. The code is tested for material non-linearity an geometric non-linearity separately using standard reference solutions. The future work is outlined as a continuity of this report.

## Nomenclature

Variables in bold are a vector or a matrix. Lower case bold variables refer to a local size, where upper case bold variables refer to a global size.

$i, j, k, l$	Tensor notation counting 1 to 3
$\alpha, \beta, \gamma, \delta$	Tensor notation counting 1 to 2
$( )^i$	Iterative form
$( \dot{ } )$	Incremental form
$( )_{,x}$	Differentiated with respect to x
$\sigma_{ij}$	Cauchy stress tensor
$\epsilon_{ij}$	Engineering strain tensor
$E_{ijkl}$	Constitutive tensor
$E$	Youngs modulus
$\nu$	Poissons ratio
$\delta$	Kroneckers delta
$J_2$	Second invariant of deviatoric stress tensor
$\sigma_e$	Effective Von Mises stress
$s_{ij}$	Deviatoric stress tensor
$\sigma_y$	Yield stress
$n$	Hardening parameter, Number of nodes for the element, incremental counter
$E_t$	Tangential Youngs modulus
$\beta$	Yielding indicator, ratio between load and displacement
<b><math>F</math></b>	Global Nodal force vector
<b><math>K</math></b>	Global Stiffness matrix
<b><math>D</math></b>	Global Nodal displacement vector
$t$	Thickness of plate
$A_0$	Initial area
$S_0$	Initial surface
$S_{\alpha\beta}$	Second Piola-Kirchhoff stress
$E_{\alpha\beta}$	Green-Lagrange strain tensor
$P_\alpha$	Surface traction in the direction of $\alpha$
$u_\alpha$	Displacement in the direction of $\alpha$

---

$L_{\alpha\beta\gamma\delta}$	Instantaneous constitutive tensor
$\mathbf{N}$	Shape functions vector
$N$	Shape functions
$\mathbf{d}_\alpha$	Local nodal displacement vector in the direction of $\alpha$
$d1_\alpha$	Displacement of node 1 in the direction of $\alpha$
$\mathbf{K}_t$	Tangential stiffness matrix
$ndof$	Number of degree of freedoms for the element
$\mathbf{N}_D$	Matrix of gradients of shape functions
$\mathbf{d}$	Local nodal displacement vector
$\mathbf{B}_{11}$	Strain-displacement vector for $E_{11}$
$\mathbf{J}$	Jacobian matrix
$\mathbf{N}_d$	Matrix of gradients of shape functions
$\xi, \eta$	Mapped coordinates
$\mathbf{d}_{xy}$	Matrix of physical coordinates
$\mathbf{\Gamma}$	Inverse of jacobian matrix
$\mathbf{S}$	Green-Lagrange stress vector
$\mathbf{B}$	Strain displacement matrix
$J$	Determinant of jacobian matrix
$GP$	Gauss point counter
$N_{GP}$	Number of Gauss point for the element
$k$	Degree of freedom counter
$\mathbf{k}_{GP}$	Local stiffness matrix for Gauss point
$W$	Weight factor of Gauss point, Width of specimen
$R$	Equilibrium correction term
$\mathbf{R}$	Nodal residual force vector
$F_{cr}$	Critical force
$H$	Height of specimen
$\mathbf{F}_n$	Current force vector
$\Delta\mathbf{F}$	Incremental force vector
$\mathbf{U}_{n-1}$	Displacement vector from last increment
$\mathbf{G}$	Internal force vector
$\mathbf{U}^i$	Iterative displacement vector
$e$	Equilibrium convergence parameter

$\mathbf{s}$	Deviatoric stress vector
$\xi$	Load factor
$c$	Constraint equation
$\mathbf{c}_{,\mathbf{U}}$	Gradient of constraint equation wrt. $\mathbf{U}$
$c_{,\xi}$	Gradient of constraint equation wrt. $\xi$
$\mathbf{U}_R^i$	Iterative displacement vector from residual part
$\Delta\mathbf{U}_F$	Incremental displacement vector from external force part
$\Delta\mathbf{U}_{F1}$	Incremental displacement vector from external force, first increment

**Abstract**

A geometric and material non-linear finite element code is built using Matlab. The theoretical derivations for building the code is outlined and explained by pseudo code. Three different solvers are introduced; the Newton Raphson method, the modified Newton Raphson method, and the arc length method. The code is tested for material non-linearity an geometric non-linearity separately using standard reference solutions. The future work is outlined as a continuity of this report.

## Preface

This report is a progress (part A) report of the work done in the period from August 1., 2011 to January 1., 2013. The report is a part of the PhD program at The Graduate School of Science and Technology at Aarhus University.

This work is addressed to the PhD comity, the supervisor of the present PhD study and the examiner.

I would like to use this opportunity to show appreciation for the help and guides provided by my supervisor Henrik Myhre Jensen. I would also like to thank Lars Erik Braüner, and my office mates Mads Krabbe, Per Christian Hyldahl, and Søren Steffensen for the daily correspondence. Besides I would like to thank Søren Nørgaard Sørensen, Aalborg University, for a good correspondence regarding coding manner.

Aarhus, January 3, 2013



---

# Contents

Nomenclature . . . . .	i
Abstract . . . . .	v
Preface . . . . .	vii
<b>1 Introduction to project</b>	<b>1</b>
<b>2 Method of solution</b>	<b>3</b>
2.1 Elasto-plastic material behaviour . . . . .	3
2.2 Finite element theory . . . . .	6
2.2.1 Implementation of an isoparametric element . . . . .	9
2.3 Numerical solution techniques . . . . .	11
2.3.1 Newton-Raphson method . . . . .	12
2.3.2 Modified Newton-Raphson method . . . . .	14
2.3.3 Arc length method . . . . .	16
<b>3 Verification</b>	<b>21</b>
3.1 Material non-linearity . . . . .	21
3.2 Geometric non-linearity . . . . .	23
<b>4 Conclusion</b>	<b>27</b>
<b>5 Future work</b>	<b>29</b>
5.1 Virtual testing . . . . .	29

CONTENTS

---

5.2 Experimental testing . . . . .	31
<b>Bibliography</b>	<b>33</b>

---

# Introduction to project

In the design of mechanical structures there is a need for having light and strong structures. One opportunity for meeting this need is the use of a light weight material like aluminium, but another option is the use of composite materials. One of the composite material option is to apply layered materials where the lay up usually is made of different materials. Each layer, called ply, are made of a reinforced material, e.g. carbon reinforced polymer. The reinforcement could be long slender continuous carbon fibres, in which the direction of orientation is crucial for the strength of the ply. This means that the strength can be orientated in a given direction where the high strength is wanted.

The good behaviour of these plies does have a backside. When the plies are in compression, the strength can be down to 60 % of the tension strength, Fleck (1997) [1]. The reduction in strength can be due to several failure mechanisms; elastic microbuckling, plastic microbuckling, fibre crushing, splitting, buckle delamination or shear band formation. One of the dominant failure modes in unidirectional reinforced polymer composite is plastic microbuckling. When plastic microbuckling occurs, the fibres tend to perform an inclined kink band of fibres that has kinked out of the original orientation. This phenomena is well known from nature where natural layered materials are performing these kink bands as well. In the paper by Paterson and Weiss (1966) [2], they experimentally observed kink band formation in phyllite (foliated rock) which

deforms in a similar manner as a unidirectional composite. Like the foliated rock, it is the shear strength and stiffness that determines when and how a kink band is formed in the composite.

The property of the plastic microbuckling failure mode is that the initiation stress is significant higher than the steady state kink band broadening stress where the instability propagates. The phenomena of propagating instabilities was reviewed by Kyriakides (1993) [3] where he characterised the failure mode in undersea pipelines.

The present work is aimed upon studying the interaction of overall structural buckling and local material instabilities by kink band formation in plate and shell structures of composite materials. The method chosen is a detailed quasi static finite element simulation of composite structures based on individual discretisation of fibres and matrix material in order to track the load/displacement response of the material. The results will be compared with a finite element formulation based on constitutive relations for effective properties of fibre composites, Jensen (1998) [4]. The discretisation of fibres and matrix material makes it possible to add cracks and holes in the structure to simulate a more direct application towards the use of this research in the industry. The possible outcome could be a method that could increase the critical buckling load for lightweight structures and thereby the possibility of making stronger and lighter composite structures.

---

## Method of solution

The method used for analysing the failure mechanics, is a non-linear finite element method. In the following the basic equations for establish a finite element code is presented. Since the problem is highly nonlinear, the code will take material non-linearity and geometric non-linearity is taken into account. Before moving to the finite element method the elasto-plastic material behaviour is described.

### 2.1 Elasto-plastic material behaviour

An essential ingredient in describing a material behaviour is the relation between strains  $\epsilon$  and stresses  $\sigma$

$$\sigma_{ij} = E_{ijkl}\epsilon_{kl} \quad (2.1)$$

where  $E_{ijkl}$  is the constitutive tensor, and the latin index notation counts from 1 to 3. For an isotropic linear elastic material the constitutive relation is

$$E_{ijkl} = \frac{E}{1 + \nu} \left( \frac{1}{2} (\delta_{ik}\delta_{jl} + \delta_{il}\delta_{jk}) + \frac{\nu}{1 - 2\nu} \delta_{ij}\delta_{kl} \right) \quad (2.2)$$

where  $E$  is Youngs modulus,  $\nu$  is Poissons ratio, and  $\delta$  is the Kronecker delta. If the material during loading becomes plastic, the constitutive relation changes with the stresses evolving. If this is the case, the material description becomes

## 2. METHOD OF SOLUTION

---

non-linear. In a non-linear analysis of material behaviour, three main ingredients are necessary; a yield criterion, a hardening rule and a flow rule. In the literature there are many different description of a yield surface. Four of them are showed in figure 2.1. The most commonly used yield surface is the

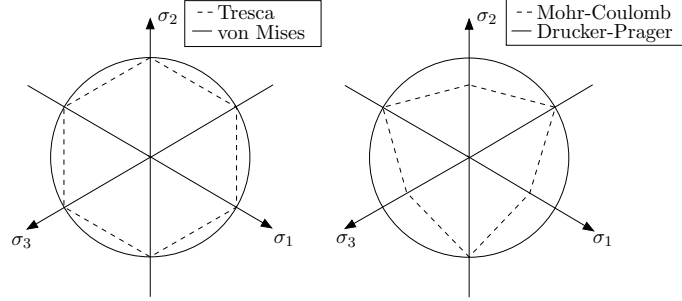


**Figure 2.1:** Yield surfaces.

Von Mises yield surface [5] given by

$$f(\sigma_{ij}) = 3J_2 = (\sigma_e)_{\max}^2 \quad (2.3)$$

where  $J_2$  is the second invariant of the deviatoric stress tensor and  $(\sigma_e)_{\max}$  is the effective Von Mises stress. The  $J_2$  stress can be written as

$$J_2 = \frac{1}{2} s_{ij} s_{ij} \quad (2.4)$$

where  $s_{ij}$  is the deviatoric stress tensor which is given by

$$s_{ij} = \sigma_{ij} - \delta_{ij} \frac{\sigma_{kk}}{3} \quad (2.5)$$

It can be seen from equation 2.4 that the effective von Mises stress  $\sigma_e$  is independent of the hydrostatic stress tensor, while only  $s_{ij}$  is contributing to  $J_2$ .

After yielding is determined by the yield criterion, the subsequent stress-strain relation must be determined. Most materials have a hardening and not a softening behaviour. The hardening law can be described in many different ways, but three well known hardening laws are

- Elastic-perfectly plastic

- Hardening slope
- Power hardening law

To simulate the physical behaviour of the material, a power hardening law is used. The power hardening law is described in a uni-axial space by

$$\epsilon = \begin{cases} \frac{\sigma}{E} & \text{for } \sigma \leq \sigma_y \\ \frac{\sigma_y}{E} \left[ \frac{1}{n} \left( \frac{\sigma}{\sigma_y} \right)^n - \frac{1}{n} + 1 \right] & \text{for } \sigma > \sigma_y \end{cases} \quad (2.6)$$

where the tangential modulus is determined by

$$E_t = \frac{d\sigma}{d\epsilon} = \left( \frac{d\epsilon}{d\sigma} \right)^{-1} \quad (2.7)$$

$$E_t = E \left( \frac{\sigma}{\sigma_y} \right)^{1-n} \quad (2.8)$$

The power hardening law was found by Borg (2003) [6] to fit the experimental data from Hsu, Vogler, and Kyriakides (1999) [7] for PEEK with an exponent  $n = 5$ .

The last ingredient in the non-linear material analysis is the flow rule. The  $J_2$ -flow theory is used as described in McMeeking and Rice (1975) [8]. The constitutive tensor  $E_{ijkl}$  in equation 2.1 is replaced with an instantaneous moduli  $L_{ijkl}$  which is an extension of equation 2.2. The instantaneous moduli is given by

$$L_{ijkl} = \frac{E}{1+\nu} \left( \frac{1}{2} (\delta_{ik}\delta_{jl} + \delta_{il}\delta_{jk}) + \frac{\nu}{1-2\nu} \delta_{ij}\delta_{kl} - \beta \frac{3}{2} \frac{E/E_t - 1}{E/E_t - (1-2\nu)/3} \frac{s_{ij}s_{kl}}{\sigma_e^2} \right) \quad (2.9)$$

where  $\beta$  is

$$\beta = \begin{cases} 1 & \text{for } \sigma_e = (\sigma_e)_{\max} \quad \text{and} \quad \dot{\sigma}_e \geq 0 \\ 0 & \text{for } \sigma_e < (\sigma_e)_{\max} \quad \text{or} \quad \dot{\sigma}_e < 0 \end{cases} \quad (2.10)$$

$(\sigma_e)_{\max}$  is the maximum effective von Mises stress. This stress is initially equal to the yield stress of the material  $\sigma_y$ , but as plasticity is evolving so is the maximum effective Von Mises stress  $(\sigma_e)_{\max}$ . The dot symbol ( $\dot{\quad}$ ) means an incremental size or a load step size. The sign of the incremental effective stress  $\dot{\sigma}_e$  determines if the material point is in a loading or a unloading state. If the material is unloading,  $\beta$  will always be 0.

## 2.2 Finite element theory

The wanted output of this analysis is the displacement  $U$  as a function of the applied force  $F$ . In the finite element method the relationship between  $F$  and  $U$  is described by

$$\mathbf{F} = \mathbf{K}\mathbf{D} \quad (2.11)$$

where  $\mathbf{F}$  is the nodal force vector,  $\mathbf{K}$  is the stiffness matrix and  $\mathbf{D}$  is the nodal displacement vector. This system of equations is an approximation of a continuous system. When capital letters is used they refer to a global quantity and when lower case letters are used they refer to a local quantity. The stiffness matrix  $\mathbf{K}$  is found using the principle of virtual work (PVW). For a planar case [9] assuming no volumetric forces

$$t \iint_{A_0} S_{\alpha\beta} \delta E_{\alpha\beta} dA_0 = \iint_{S_0} P_\alpha \delta u_\alpha dS_0 \quad (2.12)$$

where  $E$  is the Green-Lagrange strain tensor (not the Youngs modulus in this case), and  $S$  is the work conjugated second Piola-Kirchhoff stress [10].  $A_0$  and  $S_0$  denotes the area and the surface, and 0 means the PVW is formulated in the initial configuration. The Greek index notation counts from 1 to 2, so this marks the planar case. If the virtual strain tensor  $\delta E_{\alpha\beta}$  is evaluated using the total displacement, the method is called Total Lagrangian formulation [9]. If the PVW is written in incremental form, the expression after linearization and removal of constants is

$$t \iint_{A_0} \left( S_{\alpha\beta} \delta \dot{E}_{\alpha\beta} + \dot{S}_{\alpha\beta} \delta E_{\alpha\beta} \right) dA_0 = \iint_{S_0} \dot{P}_\alpha \delta u_\alpha dS_0 \quad (2.13)$$

where  $(\dot{\phantom{x}})$  is the increment. The individual parts are to be determined in the following. The total stress is

$$S_{\alpha\beta} = L_{\alpha\beta\gamma\delta} E_{\gamma\delta} \quad (2.14)$$

where  $L_{\alpha\beta\gamma\delta}$  are defined by equation 2.9. The total strain is

$$E_{\alpha\beta} = \frac{1}{2} (u_{\alpha,\beta} + u_{\beta,\alpha} + u_{\gamma,\alpha} u_{\gamma,\beta}) \quad (2.15)$$



where  $u_{\alpha,\beta}$  is the displacement in the  $\alpha$  direction differentiated with respect to  $\beta$ , and vice versa for  $u_{\beta,\alpha}$ . The virtual incremental strain is

$$\delta \dot{E}_{\alpha\beta} = \frac{1}{2} (\dot{u}_{\gamma,\alpha} \delta u_{\gamma,\beta} + u_{\gamma,\alpha} \delta \dot{u}_{\gamma,\beta}) \quad (2.16)$$

The incremental stress is defined in the same way as equation 2.14 only with the incremental strain  $\dot{E}_{\alpha\beta}$  instead of the total strain. The incremental strain is defined as

$$\dot{E}_{\alpha\beta} = \frac{1}{2} (\dot{u}_{\alpha,\beta} + \dot{u}_{\beta,\alpha} + u_{\gamma,\alpha} \dot{u}_{\gamma,\beta} + \dot{u}_{\gamma,\alpha} u_{\gamma,\beta}) \quad (2.17)$$

The last part of equation 2.13 is the virtual strain  $E_{\alpha\beta}$  which is similar to the incremental strain only with the increment switched with virtual

$$\delta E_{\alpha\beta} = \frac{1}{2} (\delta u_{\alpha,\beta} + \delta u_{\beta,\alpha} + u_{\gamma,\alpha} \delta u_{\gamma,\beta} + \delta u_{\gamma,\alpha} u_{\gamma,\beta}) \quad (2.18)$$

The displacement field within an element can be approximated by shape functions. The method of approach is to interpolate the nodal displacement  $\mathbf{d}_\alpha$  using the shape functions  $\mathbf{N}$ . The displacement field is given by

$$u_\alpha(x, y) = \mathbf{N}(x, y) \mathbf{d}_\alpha \quad (2.19)$$

where  $\mathbf{N}$  is a vector containing the shape functions

$$\mathbf{N} = \{N1 \quad N2 \quad \dots \quad Nn\} \quad (2.20)$$

The number of shape functions is given by the number of nodes for the element  $n$ . The nodal displacement vector is

$$\mathbf{d}_\alpha = \{d1_\alpha \quad d2_\alpha \quad \dots \quad dn_\alpha\}^T \quad (2.21)$$

where  $d1_1$  is the displacement of node 1 in the 1-direction and  $d1_2$  is the displacement of node 1 in the 2-direction. The same is valid for the rest of the nodal displacements. The gradients of the displacement in the 1-direction (x-direction) with respect to the 2-direction (y-direction) can be found using partial differentiation of the shape functions

$$u_{x,y} = \frac{\partial \mathbf{N}(x, y)}{\partial y} \mathbf{d}_x \quad (2.22)$$

## 2. METHOD OF SOLUTION

---

The same is applicable for the virtual and incremental displacement gradient

$$\delta u_{x,y} = \frac{\partial \mathbf{N}(x,y)}{\partial y} \delta \mathbf{d}_x \quad , \quad \dot{u}_{x,y} = \frac{\partial \mathbf{N}(x,y)}{\partial y} \dot{\mathbf{d}}_x \quad (2.23)$$

Next in line is to establish the tangent stiffness matrix  $\mathbf{K}_t$ . This is done by writing equation 2.11 in incremental form

$$\dot{\mathbf{F}} = \mathbf{K}_t \dot{\mathbf{D}} \quad (2.24)$$

This means that the left hand side (LHS) of equation 2.13 written in terms of the incremental nodal displacement  $\dot{\mathbf{D}}$ . The approach is to isolate the local incremental nodal displacement vector  $\dot{\mathbf{d}}$  when establishing the local tangent stiffness matrix  $\mathbf{k}_t$  in each element. The nodal displacement vector  $\mathbf{d}$  is an assembly of  $\mathbf{d}_1$  and  $\mathbf{d}_2$

$$\dot{\mathbf{d}} = \left\{ \dot{d}_{1,1} \quad \dot{d}_{1,2} \quad \dot{d}_{2,1} \quad \dot{d}_{2,2} \quad \dot{d}_{3,1} \quad \dot{d}_{3,2} \quad \dots \quad \dot{d}_{n,1} \quad \dot{d}_{n,2} \right\}^T \quad (2.25)$$

This means that the displacement gradients can be written as

$$\begin{Bmatrix} \dot{u}_{1,1} \\ \dot{u}_{1,2} \\ \dot{u}_{2,1} \\ \dot{u}_{2,2} \end{Bmatrix} = \begin{bmatrix} N1,1 & 0 & N2,1 & 0 & \dots & Nn,1 & 0 \\ N1,2 & 0 & N2,2 & 0 & \dots & Nn,2 & 0 \\ 0 & N1,1 & 0 & N2,1 & 0 & \dots & Nn,1 \\ 0 & N1,2 & 0 & N2,2 & 0 & \dots & Nn,2 \end{bmatrix} \dot{\mathbf{d}} \quad (2.26)$$

and in compact form as

$$\dot{\mathbf{u}}_d^{4 \times 1} = \mathbf{N}_D^{4 \times ndof} \dot{\mathbf{d}}^{ndof \times 1} \quad (2.27)$$

The same procedure can be used to evaluate the total displacement gradient  $\mathbf{u}_d$  by using the total nodal displacement  $\mathbf{d}$ . The necessary information to calculate the Green-Lagrange strain  $E_{\alpha\beta}$  and thereby the total second Piola-Kirchhoff stress  $S_{\alpha\beta}$  is now evaluated. The incremental strain  $\dot{E}_{\alpha\beta}$  is the next in line. The expression is given by equation 2.17 and as an example  $\dot{E}_{11}$  is written out

$$\dot{E}_{11} = \dot{u}_{1,1} + u_{1,1} \dot{u}_{1,1} + \dot{u}_{2,1} u_{2,1} \quad (2.28)$$

Next the incremental nodal displacement  $\dot{\mathbf{d}}$  is isolated and the expression yields

$$\dot{E}_{11} = (\mathbf{N}_D(1, :) + u_{1,1} \mathbf{N}_D(1, :) + \mathbf{N}_D(3, :) u_{2,1}) \dot{\mathbf{d}} \quad (2.29)$$

where  $(1, :)$  means the whole row of the first column. For simplicity this can be written in a compact form as

$$\dot{E}_{11} = \dot{\mathbf{B}}_{11} \dot{\mathbf{d}} \quad (2.30)$$

where  $\dot{\mathbf{B}}_{11}$  is the incremental strain-displacement vector relating the incremental nodal displacement  $\dot{\mathbf{d}}$  with the incremental normal strain in the 1-direction. The same procedure is used to determine equations 2.16 and 2.18.

### 2.2.1 Implementation of an isoparametric element

In this section an implementation of a plane isoparametric element will be presented.

The formulas derived in section 2.2 are in a physical space ie.  $xy$ -space. The same procedure can be used in an isoparametric way ie.  $\xi\eta$ -space. This is done by mapping the physical coordinates into the  $\xi\eta$  coordinates. This is done via the Jacobian matrix  $\mathbf{J}$  which is defined as

$$\mathbf{J} = \mathbf{N}_{\mathbf{d}} \mathbf{d}_{\mathbf{xy}} \quad (2.31)$$

where  $\mathbf{N}_{\mathbf{d}}$  is

$$\mathbf{N}_{\mathbf{d}} = \begin{bmatrix} N_{1,\xi} & N_{2,\xi} & \dots & N_{n,\xi} \\ N_{1,\eta} & N_{2,\eta} & \dots & N_{n,\eta} \end{bmatrix} \quad (2.32)$$

The shape functions are here given in terms of  $\xi$  and  $\eta$ .  $\mathbf{d}_{\mathbf{xy}}$  are the physical coordinates which is arranged as

$$\mathbf{d}_{\mathbf{xy}} = \begin{bmatrix} x_1 & y_1 \\ x_2 & y_2 \\ \vdots & \vdots \\ x_n & y_n \end{bmatrix} \quad (2.33)$$

where  $n$  is the number of nodes in the element. By defining a matrix  $\mathbf{\Gamma}$  as the inverse of  $\mathbf{J}$

$$\mathbf{\Gamma} = \mathbf{J}^{-1} = \begin{bmatrix} \Gamma_{11} & \Gamma_{12} \\ \Gamma_{21} & \Gamma_{22} \end{bmatrix} \quad (2.34)$$

## 2. METHOD OF SOLUTION

---

the transformation between physical gradients of deformation and mapped gradients of deformation can be written as

$$\begin{pmatrix} u_{1,1} \\ u_{1,2} \\ u_{2,1} \\ u_{2,2} \end{pmatrix} = \begin{bmatrix} \Gamma_{11} & \Gamma_{12} & 0 & 0 \\ \Gamma_{21} & \Gamma_{22} & 0 & 0 \\ 0 & 0 & \Gamma_{11} & \Gamma_{12} \\ 0 & 0 & \Gamma_{21} & \Gamma_{22} \end{bmatrix} \begin{pmatrix} u_{1,\xi} \\ u_{1,\eta} \\ u_{2,\xi} \\ u_{2,\eta} \end{pmatrix} \quad (2.35)$$

The vector on the right hand side of equation 2.35 contains the gradients of the displacements with respect to  $\xi\eta$ -coordinate system which is calculated in the same way as equation 2.26. The differentiation is done with respect to  $\xi$  and  $\eta$  instead of 1 and 2 (x and y). The local stiffness matrix  $\mathbf{k}_t$  can now be calculated as

$$\mathbf{k}_t = t \int_{-1}^1 \int_{-1}^1 \mathbf{S} \delta \dot{\mathbf{B}} + \dot{\mathbf{S}} \delta \mathbf{B} J d\xi d\eta \quad (2.36)$$

where the total stress vector  $\mathbf{S}$  is calculated from equation 2.14 and  $\delta \dot{\mathbf{B}}$  is calculated from equation 2.16 using the same procedure as equation 2.29.  $\dot{\mathbf{S}}$  is found using equation 2.17 and finally  $\delta \mathbf{B}$  is determined from equation 2.18.  $J$  is a transformation between the physical coordinates and the mapped coordinates. Finally  $J$  can be found as the determinant of the Jacobian matrix from equation 2.31

$$J = |\mathbf{J}| \quad (2.37)$$

All the terms needed to establish  $\mathbf{K}_t$  are now determined and the implementation can begin. To do the integration in equation 2.36, Gauss integration will be used. In algorithm 1 a pseudo code for establishing the local stiffness matrix  $\mathbf{k}_t$  of an isoparametric element is presented. In algorithm 1 the constitutive matrix  $\mathbf{L}$  is written in terms of the Cauchy stresses  $\boldsymbol{\sigma}$ . These stresses are known from the previous increment.  $W(GP)$  is the weight factor associated with the current Gauss point.

```

for  $GP = 1, 2, \dots, N_{GP}$  do
   $\mathbf{N}_D = \mathbf{N}_D(\xi(GP), \eta(GP))$ 
   $\mathbf{u}_d = \mathbf{N}_D \mathbf{d}$ 
   $\mathbf{S} = \mathbf{L}(\sigma) \mathbf{E}(\mathbf{u}_d)$ 
   $\dot{\mathbf{S}} = \mathbf{L}(\sigma) \dot{\mathbf{B}}(\mathbf{N}_D, \mathbf{u}_d)$ 
  for  $k = 1, 2, \dots, ndof$  do
     $\delta \mathbf{d} = \{0 \ 0 \ \dots \ 0\}^{1 \times ndof}$ 
     $\delta \mathbf{d}(k) = 1$ 
     $\delta \dot{\mathbf{B}} = \delta \dot{\mathbf{B}}(\mathbf{N}_D, \delta \mathbf{u}_d)$ 
     $\delta \mathbf{B} = \delta \mathbf{B}(\mathbf{u}_d, \delta \mathbf{u}_d)$ 
     $\mathbf{k}_{GP}(k, :) = \mathbf{S} \delta \dot{\mathbf{B}} + \dot{\mathbf{S}} \delta \mathbf{B}$ 
  end for
   $\mathbf{k}_t = \mathbf{k}_t + \mathbf{k}_{GP} t J(\xi(GP), \eta(GP)) W(GP)$ 
end for
    
```

**Algorithm 1:** The local tangent stiffness matrix  $\mathbf{k}_t$ .

## 2.3 Numerical solution techniques

Equation 2.13 is only valid if the actual increment satisfies equilibrium. Since the equation is a nonlinear equation, a linear incremental analysis would accumulate errors and drift away from the physical equilibrium path. This method is called an explicit incremental method. An alternative to this is an implicit incremental method where an equilibrium correction term is added on the right hand side of equation 2.13

$$t \iint_{A_0} \left( S_{\alpha\beta} \delta \dot{E}_{\alpha\beta} + \dot{S}_{\alpha\beta} \delta E_{\alpha\beta} \right) dA_0 = \iint_{S_0} \dot{P}_\alpha \delta u_\alpha dS_0 + R \quad (2.38)$$

where  $R$  is the equilibrium correction term (or residual) and is defined as the difference between the external virtual work and the internal virtual work

$$R = \iint_{S_0} P_\alpha \delta u_\alpha dS_0 - t \iint_{A_0} S_{\alpha\beta} \delta E_{\alpha\beta} dA_0 \quad (2.39)$$

In vector form equation 2.39 is written as

$$\mathbf{R} = \mathbf{F} \delta \mathbf{u} - \mathbf{G} \delta \mathbf{u} \quad (2.40)$$

where  $\delta \mathbf{u}$  can be omitted by setting it to 1 in turn [11]. This is similar to the calculation of the tangent stiffness matrix in algorithm 1. By applying

## 2. METHOD OF SOLUTION

---

the correction the equation will be closer to equilibrium, but not exact. To obtain a solution as close to equilibrium as wanted, several different numerical techniques are available [5]. A small part of those will be explained in the following sections. In figure 2.2 an example of the influence of equilibrium correction for a beam in axial compression with a small imperfection is shown. The equilibrium path is shown here in comparison with a solution without

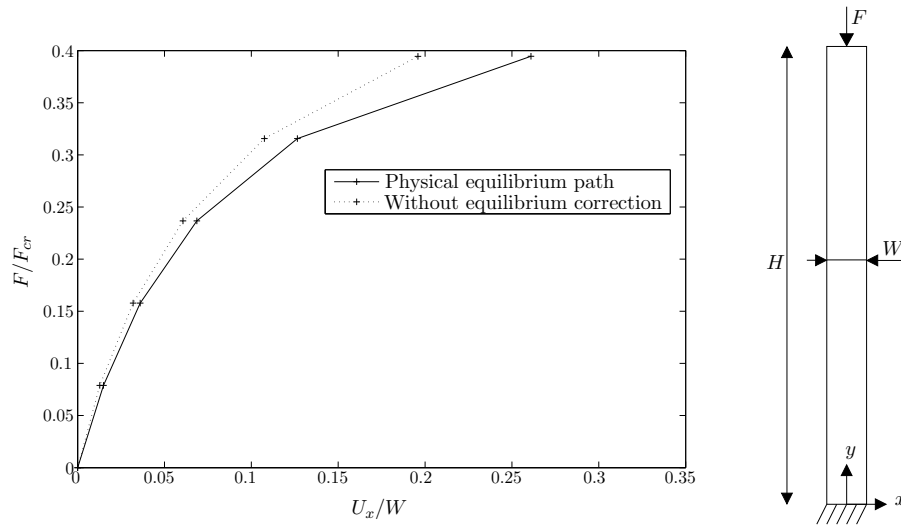


**Figure 2.2:** The effect of equilibrium correction on a beam in compression. The figure shows a vertical stress applied on the top of the beam normalized with respect to the analytical critical load as a function of the horizontal displacement at  $H/2$  normalized with respect to the width  $w$  of the beam.

equilibrium correction for large time steps. This is done in order to see the influence clearly. If smaller time steps were used the two solutions would be closer to one another. One could argue that you could might as well use small time steps and save a lot of coding but then a sudden large change in direction of the equilibrium path would be difficult to capture.

### 2.3.1 Newton-Raphson method

This equilibrium correction method is the simplest and the most widely used for a simple non-linear finite element solution procedure. The fundamentals of the method is to calculate the residual force vector and then adjust the

tangent stiffness matrix. The simplest explanation of the method is done by writing the algorithm for obtaining equilibrium in one increment. This is done in algorithm 2. The first *for*-loop counts the increments  $n$  from 1 to the

```

for  $n = 1, 2, \dots, N$  do
     $\mathbf{F}_n = \mathbf{F}_{n-1} + \Delta\mathbf{F}$ 
     $\mathbf{U}_n = \mathbf{U}_{n-1}$ 
     $\sigma_n = \sigma_{n-1}$ 
    while  $StopFlag = 0$  do
         $\mathbf{K}_t = \mathbf{K}_t(\mathbf{U}_n, \sigma_n)$ 
         $\mathbf{G} = \mathbf{G}(\mathbf{U}_n, \sigma_n)$ 
         $\mathbf{R}_n = \mathbf{F}_n - \mathbf{G}$ 
         $\mathbf{U}^i = \mathbf{K}_t^{-1}\mathbf{R}_n$ 
         $\mathbf{U}_n = \mathbf{U}_n + \mathbf{U}^i$ 
        if  $\|\mathbf{R}_n\| < e\|\Delta\mathbf{F}\| \quad \vee \quad i = i_{max}$  then
             $StopFlag = 1$ 
        end if
    end while
     $\sigma_n = \sigma_n(\mathbf{L}(\sigma_e, \mathbf{s}))$ 
end for
    
```

**Algorithm 2:** The Newton Raphson method.

total number of increment  $N$ . Next the total force  $\mathbf{F}_n$  is found from the last increment plus the incremental force  $\Delta\mathbf{F}$ . The total displacement  $\mathbf{U}$  is set to the converged displacement from the previous increment. The same is done for the Cauchy stresses, to determine the constitutive behaviour. It is recommended by Crisfield [5] to use the incremental stresses and not the iteration stresses for defining the constitutive behaviour. The iteration procedure is carried out in the *while*-loop. At first the tangent stiffness matrix  $\mathbf{K}_t$  is calculated as a function of the current displacement  $\mathbf{U}_n$  and the current stress state  $\sigma$ . The internal force vector  $\mathbf{G}$  is calculated from the same parameters. This means that  $\mathbf{K}_t$  and  $\mathbf{G}$  can be calculated at the same time. The residual force vector  $\mathbf{R}_n$  can now be determined from equation 2.40. The ingredients to solve the stiffness equation for determining the displacement for the current iteration  $\mathbf{U}_i$  are now established. This iteration displacement is added to the total displacement  $\mathbf{U}_n$ , and overwrites the previous value. The *while*-loop continues until the length of the residual  $\|\mathbf{R}_n\|$  is smaller than a fraction of

the length of the incremental force  $\|\Delta\mathbf{F}\|$ . The fraction is determined by  $e$  which could be on the order of magnitude  $10^{-4} - 10^{-6}$  [10]. Algorithm 2 can be explained further in a graphical way. In figure 2.3 an example of the force

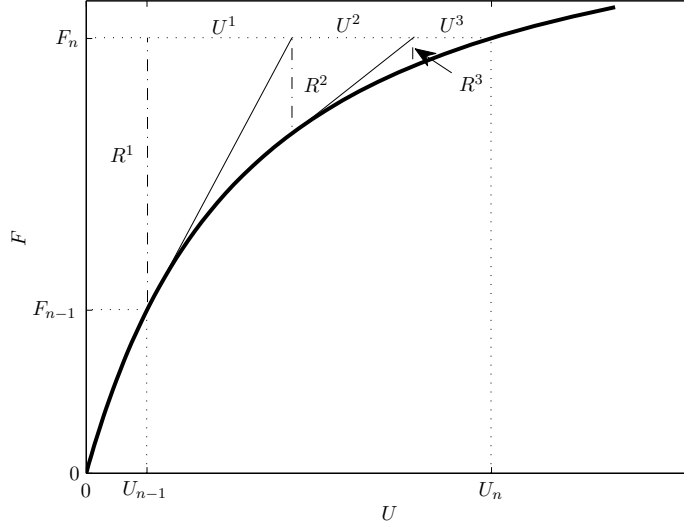


**Figure 2.3:** Graphical representation of the Newton-Raphson equilibrium correction method. The test setup is the same as in figure 2.2, and the plot shows the applied force as a function of the horizontal displacement at  $H/2$  in the x direction.

controlled Newton-Raphson algorithm is shown. The increment starts at the last established equilibrium at  $F_{n-1}$  and ends at  $F_n$  where the displacement is iteratively corrected so that equilibrium occurs at the end of the increment. It is clear that the tangential stiffness changes during the iterations which is the essence of the Newton-Raphson method.

### 2.3.2 Modified Newton-Raphson method

The procedure for the modified Newton-Raphson method is in overall the same as the one for Newton-Raphson method. The difference is in the calculation of the tangential stiffness matrix, which is calculated only in the beginning of each increment. The algorithm for the modified Newton-Raphson method is presented in algorithm 3. In the *while*-loop the inner force vector  $\mathbf{G}$  is



```
for  $n = 1, 2, \dots, N$  do  
   $\mathbf{F}_n = \mathbf{F}_{n-1} + \Delta\mathbf{F}$   
   $\mathbf{U}_n = \mathbf{U}_{n-1}$   
   $\sigma_n = \sigma_{n-1}$   
   $\mathbf{K}_t = \mathbf{K}_t(\mathbf{U}_n, \sigma_n)$   
  while  $StopFlag = 0$  do  
     $\mathbf{G} = \mathbf{G}(\mathbf{U}_n, \sigma_n)$   
     $\mathbf{R}_n = \mathbf{F}_n - \mathbf{G}$   
     $\mathbf{U}^i = \mathbf{K}_t^{-1}\mathbf{R}_n$   
     $\mathbf{U}_n = \mathbf{U}_n + \mathbf{U}^i$   
    if  $\|\mathbf{R}_n\| < e\|\Delta\mathbf{F}\| \quad \vee \quad i = i_{max}$  then  
       $StopFlag = 1$   
    end if  
  end while  
   $\sigma_n = \sigma_n(\mathbf{L}(\sigma_e, \mathbf{s}))$   
end for  
Algorithm 3: The modified Newton Raphson method.
```

updated in the same way as for the Newton-Raphson method. Since  $\mathbf{K}_t$  is updated from the equilibrium at the last increment this method will need more iterations than the Newton-Raphson method to converge. But since there is no need to calculate  $\mathbf{K}_t$  in each iteration, time is saved here.

When choosing either the full Newton-Raphson method or the modified Newton-Raphson method it is hard to say which method to choose if calculation time is essential. It is a question of time of iteration loops vs. number of iteration loops. If the equilibrium path has a small slope, the Newton-Raphson method is the fastest since the modified Newton-Raphson method needs a lot of iterations to converge. Common for both of the methods is that when the equilibrium path reaches a limit point convergence will fail. If this is the case several other methods are an option. The most obvious is to make the incremental solution displacement controlled instead of force controlled. This holds true for limit points and even snap-through problems. If snap-back behaviour will occur, this method will fail as well and techniques that can handle this type of behaviour will be presented in the following section.

### 2.3.3 Arc length method

In nonlinear finite element analysis one of the most well known techniques for tracing equilibrium when limit points, snap-through or snap back behaviour is present is the arc-length method. The method of approach is that a combined load/displacement step is controlled during equilibrium corrections via a constraint equation. This approach was first introduced by Riks in 1979 [12]. Ramm [13] reviewed numerical techniques that could trace equilibrium near limit points in 1981, and Memon and Su [14] reviewed the arc length technique development of the last two decades in 2003. In this section the bordering algorithm is introduced followed by a pseudo code explaining the implementation.

In figure 2.4 the principle of the arc length method is shown. The force

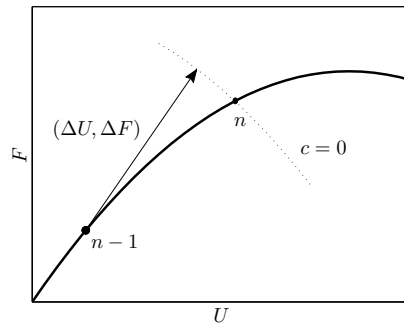


**Figure 2.4:** Principle of an increment using the arc length method. The constrain equation  $c$  is here a hypersphere marked with the dotted line.

increment is applied from the last established equilibrium at  $n-1$ , and equilibrium is searched for in the direction of the arc until the new state of equilibrium is found at  $n$ . As the figure shows, the new state is found by help of a combined load and displacement equilibrium search. The search path is defined via a constrain condition that defines the direction of the iterative equilibrium search. This means that it is necessary to satisfy the constrain condition while equilibrium iterations are executed.

For a start the equation 2.40 is written in incremental form without the

virtual displacement as

$$\mathbf{R} = \mathbf{F} - \mathbf{G} = \xi \Delta \mathbf{F} - \Delta \mathbf{G} \quad (2.41)$$

where  $\xi$  is a load factor to be established later. Since the load parameter  $\xi$  is unknown in the system of equations, another equation is to be supplied. This is the path following constraint equation and it is defined as

$$c(\Delta \mathbf{U}, \xi \Delta \mathbf{F}) = 0 \quad (2.42)$$

The constraint equation connects the current displacement  $\Delta \mathbf{U}$  to the current load increment  $\xi \Delta \mathbf{F}$ . The linearised combined equilibrium and constraint equation that needs to be satisfied can be written as

$$\mathbf{R} + \mathbf{R}^i = \mathbf{0} \quad (2.43)$$

$$c + c^i = 0 \quad (2.44)$$

where the superscript  $i$  indicates the iteration. Since the independent variables of the problem are  $\mathbf{U}$  and  $\xi$ , the linearised equation take the form

$$-\frac{\partial \mathbf{R}}{\partial \mathbf{U}} \mathbf{U}^i - \frac{\partial \mathbf{R}}{\partial \xi} \xi^i = \mathbf{R} \quad (2.45)$$

$$-\frac{\partial c}{\partial \mathbf{U}} \mathbf{U}^i - \frac{\partial c}{\partial \xi} \xi^i = c \quad (2.46)$$

where  $\partial \mathbf{R} / \partial \mathbf{U} = -\mathbf{K}_t$  and  $\partial \mathbf{R} / \partial \xi = \Delta \mathbf{F}$ . If the notation  $\partial c / \partial \mathbf{U} = \mathbf{c}_{,U}^T$  and  $\partial c / \partial \xi = c_{,\xi}$  is introduced, equations 2.45 and 2.46 can be written as

$$\begin{bmatrix} \mathbf{K} & -\Delta \mathbf{F} \\ -\mathbf{c}_{,u}^T & -c_{,\xi} \end{bmatrix} \begin{Bmatrix} \mathbf{U}^i \\ \xi^i \end{Bmatrix} = \begin{Bmatrix} \mathbf{R} \\ c \end{Bmatrix} \quad (2.47)$$

The easy way of solving equation 2.47 is to solve it in parts. The first equation solved for  $\mathbf{U}^i$  can be written as

$$\mathbf{U}^i = \mathbf{K}^{-1} \mathbf{R} + \xi^i \mathbf{K}^{-1} \Delta \mathbf{F} \quad (2.48)$$

which can be split in a contribution from the residual and one from the incremental force as

$$\mathbf{U}^i = \mathbf{U}_R^i + \xi^i \Delta \mathbf{U}_F \quad (2.49)$$

## 2. METHOD OF SOLUTION

---

Using equation 2.47 the second equation can be written as

$$\xi^i = -\frac{\mathbf{c}_{,U}^T \mathbf{U}_R^i + c}{\mathbf{c}_{,U}^T \Delta \mathbf{U}_F + c_{,\xi}} \quad (2.50)$$

which can be inserted in equation 2.49 for the iterative displacement with combined equilibrium correction and satisfaction of the constraint equation. Equation 2.50 is the general expression for the load parameter  $\xi^i$ .

The definition of the constraint equation is individual for every type of arc length method. It can be a hyperplane, an updated hyperplane, a hypersphere and so on. If a linear constraint is used, a hyperplane is orthogonal to the combined displacement/load increment. This correspond to the condition that the iteration load/displacement is orthogonal to the incremental load/displacement and expressed as

$$c = (\Delta \mathbf{U}, \Delta \mathbf{F}) \cdot (\mathbf{U}^i, \mathbf{F}^i) = 0 \quad (2.51)$$

where the dot symbol represents a suitable scalar product in the load/displacement space. To do this a scalar  $\beta$  is introduced as a flexibility parameter representing the ratio between the load and the displacement space. The constraint equation can then be written as

$$(\Delta \mathbf{U}, \Delta \mathbf{F}) \cdot (\mathbf{U}^i, \mathbf{F}^i) = \Delta \mathbf{U}^T \mathbf{U}^i + \beta^2 \Delta \mathbf{F}^T \mathbf{F}^i \quad (2.52)$$

Equation 2.49 can now be inserted and if a fixed hyperplane is used the load parameter can be determined as

$$\xi^i = -\frac{\Delta \mathbf{U}^T \mathbf{U}_R^i}{\Delta \mathbf{U}^T \Delta \mathbf{U}_{F1} + \beta^2 \Delta \mathbf{F}^T \Delta \mathbf{F}_1} \quad (2.53)$$

where the subscript  $F1$  and  $1$  returns to the first iteration in the load step in which the hyperplane is fixed during iteration. When doing this, one must also remember to use  $\Delta \mathbf{U}_{F1}$  instead of  $\Delta \mathbf{U}_F$  in equation 2.49. It is shown by Crisfield [5] in 1981 that it is preferable to fix the incremental length in displacement space, which means that  $\beta = 0$ . This is done in a pseudo code in algorithm 4 where a fixed hyperplane arc length algorithm is presented. In the algorithm it can be seen that the tangent stiffness matrix  $\mathbf{K}_t$  is calcu-

---

```

while  $U < U_{max} \quad \wedge \quad n < n_{max}$  do
   $\mathbf{K}_t = \mathbf{K}_t(\mathbf{U}_n, \sigma_n)$ 
   $\Delta \mathbf{U}_{F1} = \mathbf{K}_t^{-1} \Delta \mathbf{F}$ 
   $\xi = \|\Delta \mathbf{U}\| / \|\Delta \mathbf{U}_{F1}\|$ 
   $\Delta \mathbf{U} = \xi \Delta \mathbf{U}_{F1}$ 
  while  $StopFlag = 0$  do
     $\Delta \mathbf{G} = \mathbf{G}(\mathbf{U}_{n-1} + \Delta \mathbf{U}) - \mathbf{F}_{n-1}$ 
     $\mathbf{R} = \xi \Delta \mathbf{F} - \Delta \mathbf{G}$ 
     $\mathbf{U}_R^i = \mathbf{K}_t^{-1} \mathbf{R}$ 
     $\xi^i = -\Delta \mathbf{U}^T \mathbf{U}_R^i / \Delta \mathbf{U}^T \Delta \mathbf{U}_{F1}$ 
     $\mathbf{U}^i = \mathbf{U}_R^i + \xi^i \Delta \mathbf{U}_{F1}$ 
     $\Delta \mathbf{U} = \Delta \mathbf{U} + \mathbf{U}^i$ 
     $\xi = \xi + \xi^i$ 
    if  $\|\mathbf{R}\| < e \|\Delta \mathbf{F}\| \quad \vee \quad i = i_{max}$  then
       $StopFlag = 1$ 
    end if
  end while
   $\sigma_n = \sigma_n(\mathbf{L}(\sigma_e, \mathbf{s}))$ 
   $\mathbf{U}_n = \mathbf{U}_{n-1} + \Delta \mathbf{U}$ 
   $\mathbf{F}_n = \mathbf{F}_{n-1} + \xi \Delta \mathbf{F}$ 
end while

```

**Algorithm 4:** The arc-length method.

lated outside of the iteration loop. This corresponds to the modified Newton-Raphson method and this has been found to increase the robustness of the algorithm[10]. The initial value in each increment of the load parameter  $\xi$  is calculated from the length of the displacement vector  $\|\Delta \mathbf{U}\|$  from the previous increment divided with the length of the displacement vector from the initial load step in the current increment  $\|\Delta \mathbf{U}_{F1}\|$ . The iterative load parameter  $\xi^i$  is calculated with a fixed incremental length in displacement space, i.e.  $\beta = 0$ . In the end of the algorithm the total applied force is calculated using the load parameter  $\xi$ . In figure 2.5 the principle of a load step is shown using algorithm 4. The incremental and iterative force/displacement is shown with the orthogonal constraint.

Since the arc length method is a sort of force controlled method, a different approach is needed if a displacement controlled method is wanted. This can

## 2. METHOD OF SOLUTION

---

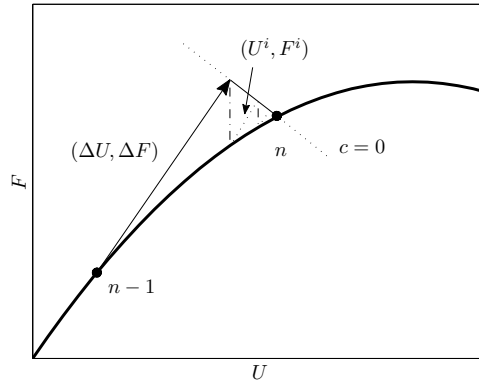


**Figure 2.5:** An incremental load step using the arc length method using a fixed hyperplane constraint on the load/displacement space.

be done by the use of Lagrange multipliers to enforce constraints. When using this method, prescribed relations are made via multipoint constraints (MPC's). For further explanation see Cook [15].

---

## Verification

To check if the finite element code is working properly, several standard examples are checked against known results. The material non-linearity and geometrically non-linearity is tested separately to keep the two features separated.

### 3.1 Material non-linearity

In the finite element code, the stresses are calculated at the Gauss points. The stresses are then used to determine the constitutive tensor at each Gauss point individually. The constitutive tensor is afterwards used in the next load step to establish the stiffness matrix.

The material non-linearity is in the following checked to see if the input stress/strain relation is the same as the measured one during loading. In figure 3.1 three curves are shown to compare the input power hardening law, the measured stress at a Gauss point, and the externally applied stress. The test specimen is a simply supported square exposed to an equally distributed unidirectional stress where the incremental method is the arc length method. The power hardening law used is equation 2.6 with the hardening exponent  $n = 10$ . The three curves are almost identical which was expected.

Since the finite element code should be able to handle unloading as well as loading, a hardening rule is introduced and checked. To test this a simply supported square is again used as a reference with an isotropic hardening rule.

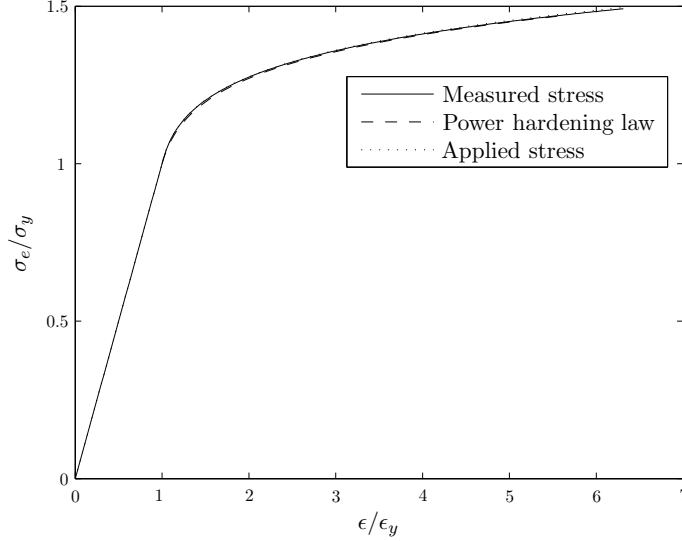


**Figure 3.1:** Comparison of the input power hardening law, the measured effective Von Mises stress at a Gauss point, and the externally applied stress. The test specimen is a simply supported square in equally distributed tension.

The tracking of the stress/strain relation for a single Gauss point is shown in figure 3.2. The first path, ①, shows the elastic loading in tension. The second path, ②, shows the material in yielding following the power hardening law with  $n = 10$ . When the strain exceeds a certain limit, the unloading begins following the third path, ③. The unloading is done using the elastic Young's modulus. Since isotropic hardening is used, unloading continues until the maximum effective stress  $(\sigma_e)_{max}$  is reached in compression. When this happens, the tracking continues on the fourth path, ④, using the power hardening law which in this case is the same in compression.



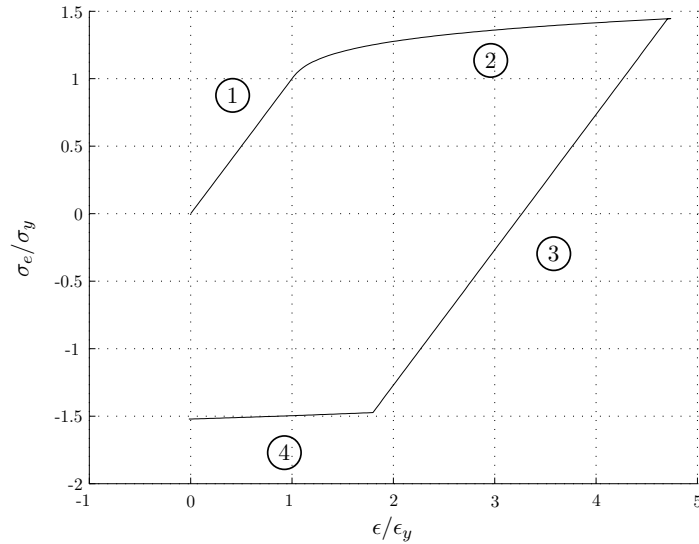


**Figure 3.2:** Tracking of loading and unloading of a square in stress/strain space using isotropic hardening.

## 3.2 Geometric non-linearity

To verify the geometric non-linearity, two different examples are used; a beam in compression, and a beam in bending.

The purely elastic beam in compression with a small imperfection can be seen in figure 3.3. The applied force  $F$  normalised with respect to the analytical critical force  $F_{cr}$  is tracked as a function of the displacement  $U$  normalised with respect to the width  $W$  of the beam. The curve seems to break off at approximately the analytical critical load which was expected. Afterwards a stable post buckling path is evolving. As the bending of the beam is evolving the bending stiffness is seen in the curve as an increasing slope.

The second test example is a beam in bending. The geometry and setup is the same as Lyons and Holsgrove (1989) [16]. They made a numerical reference solution to a straight beam in bending by a moment, bending by a force, and compression. In figure 3.4 a comparison with the work done by Lyons and

### 3. VERIFICATION

---

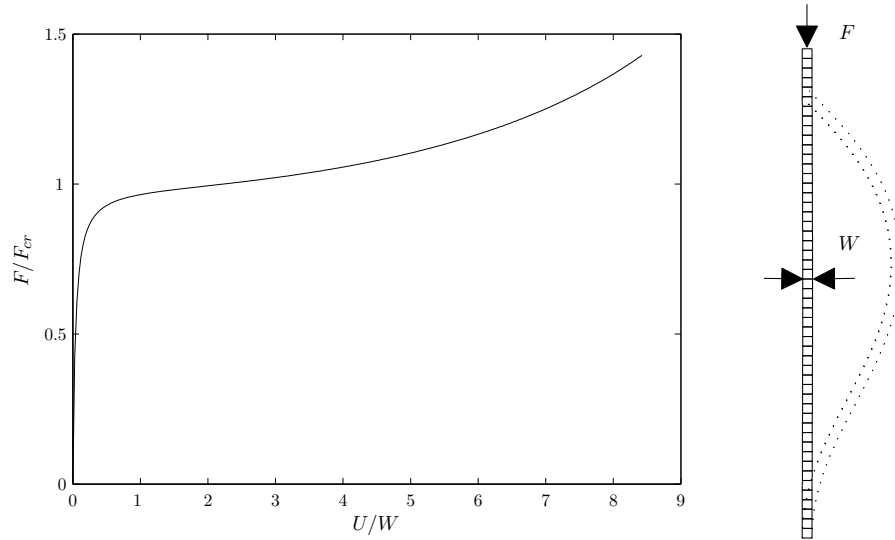


**Figure 3.3:** A vertical force  $F$  applied and normalized with respect to the analytical critical force  $F_{cr}$  as a function of the horizontal displacement  $U$  normalised with respect to the width  $W$  of the beam.

Holsgrove for a fixed beam in bending by a force is shown. The solver used for this analysis is the Newton-Raphson method. As in the reference solution, 10 fixed load steps are used. The undeformed and the deformed configuration of the beam can be seen in figure 3.5.

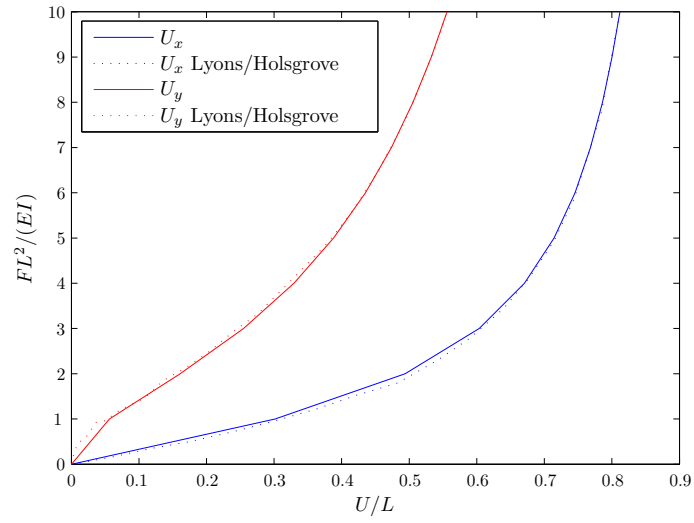


**Figure 3.4:** Comparison with a reference solution to a beam in bending by a force.

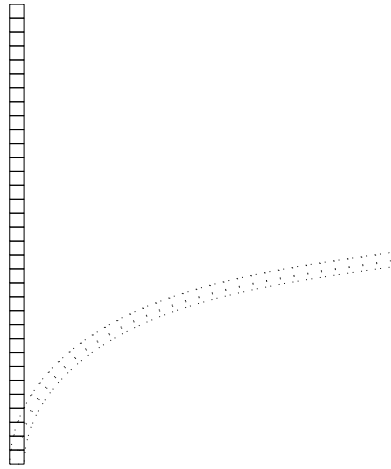


**Figure 3.5:** Undeformed and deformed configuration of the beam in bending by a force.



---

## Conclusion

The present study is aimed at making a finite element code capable of including geometric and material non-linearity for analysing unidirectional fibre composites. This is done by the use of Matlab as the coding language. The finite element code is made of raw code except for the equation solver where the built in sparse solver is used in Matlab.

Three different nonlinear solvers are presented; the Newton-Raphson method, the modified Newton-Raphson method, and the arc length method. A pseudo code is presented for each of them as a tool for implementation and to support the theoretical derivation of the methods.

To verify the nonlinear solvers and the code in general, different benchmark examples are used as a reference frame for testing the code. First the material non-linearity is tested to see if the non-linear material model that has been applied can be measured as the loading is evolving. A power hardening law is used as an example and this is plotted against the externally applied stress and the measured stress at a single Gauss point. As expected the three curves were almost identical. The small deviation could be due to the fact that the stress update is a forward Euler method but this can be reduced by using smaller time steps. The second test is a loading/unloading test where the structure is loaded above yielding in tension and thereafter unloaded and compressed where yielding occurs again. The stress/strain curve was tracked for a single Gauss point using an isotropic hardening law and the result is convincing.

#### 4. CONCLUSION

---

The geometric non-linearity is checked in two situations; a beam in compression, and a beam in bending. The beam in compression is checked against the analytical critical load. The displacement of the mid-node of the beam is tracked as a function of the applied load and the result is promising. The bending of the beam in the second geometric non-linear test was checked against a reference solution from a NAFEMS report [16]. The displacement of the node at the tip of the beam is plotted against the applied load. The curves from the reference solution is compared, and the solutions are in very good agreement.

---

## Future work

The future work will be addressed in two different directions. The first one will be a further verification of the finite element code and a virtual testing on different specimens. The second one will be experimental tests that will be conducted at the University of Michigan in USA at the Aerospace Engineering department with supervising by Anthony M. Waas.

### 5.1 Virtual testing

First of all the finite element code must be verified against already published results. A suggestion is to verify the results published by Jensen (1998) [4]. In his paper a constitutive relation for effective properties of a 2D fibre composite was used for determining the applied stress as a function of the fibre rotation. This is done in order to test if the finite element code is capable of tracking the plastic microbuckling where a kink band is shaped.

When the plastic microbuckling is verified, the next test can be conducted. This will be a study of the slenderness effect on the critical buckling load. This is interesting because when a long beam is compressed the imperfection does not have a big influence on the critical buckling load, but when a short beam is compressed it is highly imperfection sensitive. The idea is to have a fixed imperfection and then make the same study as Jensen (1998) just with the slenderness as a variable. A graph of the critical buckling load as a function

## 5. FUTURE WORK

---

of the length of the specimen can be drawn to see the comparison of a long beam vs. a short beam to see the slenderness influence. The same procedure can then be made with several different imperfections to see what influence the imperfection size have.

The next thing that could be interesting to test is a structure with holes and notches. Fleck (1997) [1] did this in his review paper but further development of his work is an option. What could be interesting to investigate is something like figure 5.1. A plate with geometry imperfections like holes or

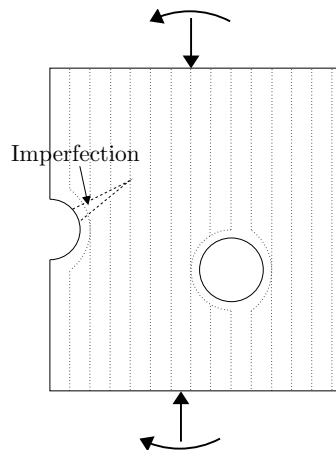


**Figure 5.1:** Hole and notch.

notches with fibre misalignment different places in the plate should be analysed. Parameters like the location of the misalignment and the location of the hole and notch could be interesting to look into. Another thing could be the layup of the fibres near the hole. Is the best thing a drilled hole or a layup with continues fibres around the hole? Different load scenarios with moment, normal force and shearing force could be applied to see the difference in the load scenario.

The last thing that could be interesting to test is plastic microbuckling in 3 dimensions. How will the kink brand develop and how will the broadening take place? How will the imperfection influence the critical buckling load?

There are several things that can be tested using the finite element code. This is just some ideas that could be interesting to investigate.



## 5.2 Experimental testing

The choice of making experimental testing by help of Anthony M. Waas was done because he have a great experience in testing composite materials. In 2004 he was a part of an experiment where they tested composite materials in off axis compression [17]. The equipment they used can be used in the present experiments as well. The following ideas is experimental tests that should help verify the numerical calculations.

First of all a compression test of a plate with a controlled fibre waviness could be conducted. The controlled fibre waviness needs to be quite large, while it is properly hard to make a composite plate with a controlled small imperfection because of the small length scale. The numerical calculations is made with 2D elements, so this means that the compression test must be made in a way so that the plate is fixed against buckling out of the plane like in [17]. The reason for making this test is to track if the kink band broadening is developing similar to the numerical calculations. When a large imperfection is used, the limit point where the critical load is found is not so sharp and no snap back behaviour will occur. This makes a displacement controlled test possible.

The numerical calculations made with the slenderness influence on the beam needs to be verified with experiments. A controlled imperfection could be introduced in this test as well. Again the result would be a plot of the critical load as a function of the length of the test specimen.

Depending on what is possible to construct, the plate with a hole and a notch could be tested. Many different layups of the unidirectional composite could be tested near the hole and the notch. The geometry could be extended to include cracks as well.



---

## Bibliography

- [1] N.A. Fleck. Compressive failure of fibre composites. *Advances in Applied Mechanics*, 33:43–117, 1997.
- [2] M.S. Paterson and L.E. Weiss. Experimental deformation and folding in phyllite. *Geological Society of America*, 77(4):343–374, 1966.
- [3] S. Kyriakides. Propagating Instabilities in Structures. *Advances in Applied Mechanics*, 30:67–189, 1993.
- [4] H.M. Jensen. Analysis of compressive failure of layered materials by kink band broadening. *International Journal of Solids and Structures*, 36(23):3427–3441, 1999.
- [5] R. De Borst, M. Crisfield, J. Remmers, and C. Verhoosel. *Nonlinear Finite Element Analysis of Solids and Structures*. Wiley Series in Computational Mechanics. Wiley, 2012.
- [6] U. Borg. Tryk og trækstyrke af fiberlaminat med porøsitet. Master’s thesis, DTU, 2003.
- [7] SY Hsu, TJ Vogler, and S Kyriakides. On the axial propagation of kink bands in fiber composites: Part II analysis. *International journal of Solids and Structures*, 36(4):575–595, 1999.

## BIBLIOGRAPHY

---

- [8] R.M. McMeeking and J.R. Rice. Finite-element formulations for problems of large elastic-plastic deformation. *International Journal of Solids and Structures*, 11(5):601 – 616, 1975.
- [9] K.J. Bathe. *Finite element procedures*. Prentice Hall, 1996.
- [10] S. Krenk. *Non-linear Modeling and Analysis of Solids and Structures*. Cambridge University Press, 2009.
- [11] H. M. Jensen. A simple finite element for non-linear material behaviour. Lecture notes, 2010.
- [12] E. Riks. An Incremental Approach to the Solution of Snapping and Buckling Problems. *International Journal of Solids and Structures*, 15(7):529–551, 1978.
- [13] Ramm, E. (Edited by Wunderlich, W., Stein, E., Bathe, K-J.). Strategies for tracing the nonlinear response near limit points. In *2nd US-Europe Workshop, Bochum, Germany*, pages 63–89. Springer, 1981.
- [14] Bashir-Ahmed Memon and Xiao-zu Su. Arc-length technique for non-linear finite element analysis. *Journal of Zhejiang University. Science*, 5(5):618–28, May 2004.
- [15] R.D. Cook. *Concepts and applications of finite element analysis*. Wiley, 2001.
- [16] P. Lyons and S. Holsgrove. *Finite Element Benchmarks for 2D and Axisymmetric Shells Involving Geometric Nonlinearity*. NAFEMS report P10. NAFEMS, 1989.
- [17] Amit G. Salvi, Anthony M. Waas, and Ari Caliskan. Specimen size effects in the off-axis compression test of unidirectional carbon fiber tow composites. *Composites Science and Technology*, 64(1):83–97, 2004.

---

# Jens Lycke Wind: Composite materials in compression, 2013